AGU PUBLICATIONS

JGR

Journal of Geophysical Research: Atmospheres

RESEARCH ARTICLE
10.1002/2014JD022975

Key Points:
- Develop ET-Tagging to separately track moisture of transpiration and evaporation
- Apply and demonstrate the method to the subtropical Poyang Lake region
- Land-air interactions control the individual contributions to precipitation

Correspondence to:
J. Wei,
jianhui.wei@kit.edu

Citation:
Wei, J., H. R. Knoche, and H. Kunstmann (2015), Contribution of transpiration and evaporation to precipitation: An ET-Tagging study for the Poyang Lake region in Southeast China, *J. Geophys. Res. Atmos.*, *120*, 6845–6864, doi:10.1002/2014JD022975.

Received 11 DEC 2014
Accepted 1 JUL 2015
Accepted article online 4 JUL 2015
Published online 29 JUL 2015

Contribution of transpiration and evaporation to precipitation: An ET-Tagging study for the Poyang Lake region in Southeast China

Jianhui Wei[1,2], Hans Richard Knoche[1], and Harald Kunstmann[1,2]

[1]Institute of Meteorology and Climate Research (IMK-IFU), Karlsruhe Institute of Technology, Campus Alpin, Garmisch-Partenkirchen, Germany, [2]Institute of Geography, University of Augsburg, Augsburg, Germany

Abstract In this study, a regional climate model-based evapotranspiration tagging (ET-Tagging) algorithm has been applied for the first time over Southeast China. Fifteen month simulations (October 2004 to December 2005) were performed to investigate where and to which extent the tagged evapotranspired water from the Poyang Lake region returns to the land surface as precipitation. The contributions of direct evaporation and transpiration were estimated separately using an extended ET-Tagging partitioning algorithm. In 2005, the contribution of moisture originating from the Poyang Lake region to the local annual precipitation in Southeast China reaches a value of up to 1.2%. A maximum contribution of 6% is found near the Poyang Lake region in August. In 2005, 69% of total tagged precipitation originates from direct evaporation of water whereas 31% from transpiration. In winter, precipitation originating from transpired moisture only accounts for around 10% of the total tagged precipitation, but in the summer season the contribution of transpiration increases up to 50%. To explore the source-target relations under consideration of the respective precipitation regime, we introduce source-specific precipitation efficiencies. For the period under investigation, the efficiency for direct evaporation generally dominates, except during the comparatively dry August and in the winter months. Our study shows that the location and the magnitude of tagged precipitation show large spatial and temporal variations. The comprehensive interactions between land surface characteristics and synoptic weather conditions control the annual cycle of the individual contributions to precipitation, emphasizing the important impacts of vegetation cover and land use on the atmospheric hydrological cycle.

1. Introduction

Evapotranspiration (ET) and precipitation (P) are the two essential components of the hydrological cycle, which link the terrestrial and atmospheric hydrological processes. Their relationship accordingly is crucial for land-atmosphere interaction studies. By now, it is well established that changes to the land surface can significantly alter the atmospheric branch of the hydrological cycle [*Huntington*, 2006] and can further modify climate variability [*Karl and Trenberth*, 2003; *Seneviratne et al.*, 2006]. The relationship between ET and P is highly uncertain and shows spatial and temporal variations depending on the regional climate regime [*Seneviratne et al.*, 2010].

Atmospheric moisture tracking with water vapor tracers [*Sodemann et al.*, 2009; *Knoche and Kunstmann*, 2013; *Winschall et al.*, 2014] in numerical models is a way to characterize the regional precipitation response to local evapotranspiration. The main idea is the consideration of a secondary atmospheric hydrological cycle of those tracers [*Sodemann et al.*, 2009]. *Joussaume et al.* [1986] and *Koster et al.* [1986] introduced the concept of tagging algorithm and implemented the algorithm in a global circulation model for investigating global sources of local precipitation. This model was applied by *Druyan and Koster* [1989] in order to identify sources of Sahel precipitation in dry and wet seasons. In 1999, *Numaguti* [1999] used the Center for Climate System Research/National Institute for Environmental Studies Atmospheric General Circulation Model (GCM) in conjunction with water vapor tracers to examine the origin of precipitation water over the Eurasian continent and to investigate time scale and frequency of recycling processes. Following the same idea, *Bosilovich and Schubert* [2002] summarized this concept and extended the Goddard Earth Observing System GCM.

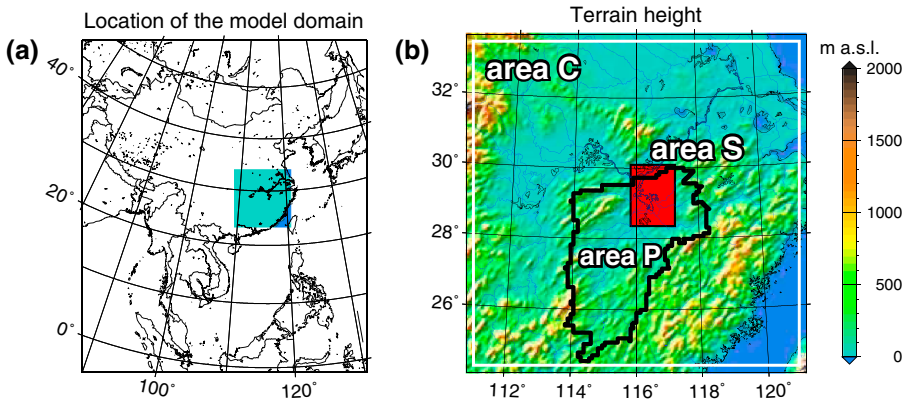

Figure 1. (a) Model domain setup. (b) Terrain height (m above sea level) as used in the MM5 model with a horizontal resolution of 4.5 km. Rivers, lakes, and the ocean are shown in blue. The red-shaded area (area S: the Poyang Lake region) marks the source region where evapotranspired water is tagged. The black frame (area P: the Poyang Lake basin) and the large white rectangle (area C: the model domain except a small boundary zone, nearly representing Southeast China) indicate different target regions where the tagged precipitation is analyzed.

The extended Finite Volume GCM [*Bosilovich*, 2003] was used for studies on regional [*Bosilovich and Chern*, 2006] and global scales [*Bosilovich et al.*, 2005]. Recently, regional models with high resolution receive increasing attention due to the fast development in high-performance computation. This allows researchers to focus on estimates of sources of precipitation on different temporal scales. Event-based rainfall was investigated by using mesoscale models, for example, the High-Resolution Model HRM [*Sodemann et al.*, 2009] and the COSMO model [*Winschall et al.*, 2014]. In addition, *Knoche and Kunstmann* [2013] conducted 2 month simulations using the Fifth-Generation Mesoscale Model MM5 with a tagging extension to show the evolution of the tagged moisture field and to reveal details of the transport on a monthly scale. Comprehensive overviews of atmospheric moisture tracking and precipitation recycling are given in *Eltahir and Bras* [1996], *Burde and Zangvil* [2001], and *Gimeno et al.* [2012].

Our evapotranspiration study focuses on the Poyang Lake (29°N, 116°E) area, which is located in the center of Southeast China (see Figure 1). Poyang Lake is the largest freshwater lake in China covering on average an area of 3500 km^2 in a hydrologically normal year. The fluctuation of the lake area is controlled by discharges from the five tributaries in the catchment and by outflow into the Yangtze River [*Ye et al.*, 2011]. From a hydrological perspective, it is an important flood storage and detention area along the Yangzte River [*Shankman et al.*, 2012]. To protect its abundant biodiversity, Poyang Lake National Nature Reserve adjacent to the Yangtze River provides habitats for migratory birds and endangered white cranes [*Jiao*, 2009].

Recently, changes in the Poyang Lake level and the associated impacts on water supplies and ecosystems have been investigated extensively on the aspects of both regional climate change and human activities [*Zhang et al.*, 2014a]. *Liu et al.* [2013] detected a decreasing trend of the lake size, based on the analysis of satellite images and hydrological data. In 2006, an abrupt change of the Poyang Lake was identified and directly related to the start of regular operation of the Three Gorge Dams in the same year [*Zhang et al.*, 2012; *Liu et al.*, 2013; *Gao et al.*, 2013]. The dam operation induces a decreasing discharge in the downstream Yangtze River at the Poyang Lake outlet, which enhances the outflow of the Poyang Lake to the Yangtze River, particularly during the dry season. Solving the problem of "water loss" or at least minimizing these impacts on the Poyang Lake and its surrounding wetlands is of great concern for local governments [*Jiao*, 2009; *Zhang et al.*, 2012]. Many studies have addressed this issue by investigating the land hydrological and hydraulic processes of the Poyang Lake area [*Zhang et al.*, 2012; *Ye et al.*, 2013; *Lai et al.*, 2014; *Zhang et al.*, 2014a]. However, only very few studies attempt to shed light on the water loss issue in terms of the atmospheric branch of the hydrological cycle, especially, the fate of water evapotranspired from the Poyang Lake and its surrounding wetlands in the atmosphere.

Precipitation in China generally shows a large variability in spatial and temporal distribution, and changes in the frequency and intensity of extremes due to climate change [*Liu et al.*, 2005]. In the Poyang Lake basin, the frequency of extreme events such as heavy precipitation, floods, and droughts has been shown to increase due to changes in the large-scale circulation [*Zhang et al.*, 2008, 2011; *Shankman et al.*, 2006] and due to

intensive human activities [*Ye et al.*, 2013] and further result in serious hydrological, ecological, and economic consequences [*Zhang et al.*, 2014a, 2014b; *Xie et al.*, 2013; *Deng et al.*, 2011]. Land-atmosphere interactions in the Poyang Lake region and their possible influence over Southeast China can be inferred from past research using analytical methods on global scales [*Trenberth and Guillemot*, 1995; *Trenberth*, 1998, 1999] and for the whole of China [*Simmonds et al.*, 1999; *Zhou and Yu*, 2005].

Previous studies have stated that more than 40% of precipitation in China is of continental origin [*Bosilovich*, 2002; *Yoshimura et al.*, 2004; *van der Ent et al.*, 2010; *Goessling and Reick*, 2011, 2013; *van der Ent et al.*, 2014]. Using the Water Accounting Model, *van der Ent et al.* [2010] found that 80% of China's water resources depends on terrestrial evaporation from the Eurasian continent. Oceanic evaporationsheds (sources) for precipitation in China covers the Atlantic Ocean westward of Europe, the Bay of Bengal, and the South China Sea [*van der Ent and Savenije*, 2013]. Additionally, *Wei et al.* [2012a] investigated the water vapor sources for the Yangtze River Valley rainfall with a quasi-isentropic back trajectory method, using MERRA reanalysis data [*Rienecker et al.*, 2011]. It is shown that the major moisture source for the Yangtze River Valley is temporally varying between the Bay of Bengal, the South China Sea, and the western Pacific.

The local recycling over the Yangtze River Valley is controlled by rainfall and circulation changes [*Wei et al.*, 2012a]. Recently, *Wang-Erlandsson et al.* [2014] and *van der Ent et al.* [2014] depicted the contrasting roles of interception and transpiration in the hydrological cycle in the context of moisture recycling and stressed the potential influence of the land surface on the hydrological cycle. By analyzing the precipitationsheds, *Keys et al.* [2012] and *Keys et al.* [2014] found that North China and East China are highly vulnerable to land use change. *Bagley et al.* [2012] indicated a negative affect of land use change on potential crop yields due to a shortage of moisture sources for the breadbasket regions, e.g., North China. An enhancement of moisture recycling has also been attributed to irrigation [*Tuinenburg et al.*, 2012; *Wei et al.*, 2012b; *Lo and Famiglietti*, 2013]. Therefore, under the conditions of the complex mountainous terrain and the monsoon system in Southeast China, both land surface characteristics and atmospheric characteristics must be taken into account in the studies of moisture tracking. It has been shown that evapotranspiration (transpiration and evaporation) is considerably affected by land surface characteristics like water bodies, soil, and vegetation [*Lawrence et al.*, 2007; *Wang and Dickinson*, 2012; *Wang-Erlandsson et al.*, 2014]. Two key atmospheric features, which are the presence of the directional wind shear and the frequency of the strong moist convection [*Goessling and Reick*, 2013; *van der Ent et al.*, 2013], should be considered in the studies of moisture tracking as well. Consequently, as a next step a detailed atmospheric model including a sophisticated land surface model for moisture tracking should be employed to gain more insight into the dynamical and hydrological processes.

Following this idea, we apply a regional climate model (RCM) with an implemented evapotranspiration tagging (ET-Tagging) algorithm [*Knoche and Kunstmann*, 2013] in this study. The model allows to tag the moisture evapotranspired from a certain region into the atmosphere and to track it until returning to the land surface as precipitation. The ET-Tagging algorithm has been originally implemented by *Knoche and Kunstmann* [2013] into the Fifth-Generation Mesoscale Model (MM5) and is extended further in this study. Individual evaporation and transpiration fluxes are calculated within a sophisticated land surface scheme (Oregon State University Land Surface Model OSU-LSM) in the regional climate model (MM5). They represent different dynamical effects of land surface characteristics and of hydrological processes [*Jacobs and De Bruin*, 1992; *Sewall et al.*, 2000; *Wang and Dickinson*, 2012; *Wang-Erlandsson et al.*, 2014; *van der Ent et al.*, 2014].

The model is applied for the first time in the mountainous, subtropical monsoon region of Southeast China. To investigate the relative importance of evaporation and transpiration processes in the regional hydrological cycle and the corresponding impact on land-atmosphere interaction, the total evapotranspiration is split into direct evaporation (consisting of evaporation from inland water bodies, evaporation from the top soil layer, and evaporation of precipitation intercepted by the canopy) and transpiration, which are then tracked separately. The objectives of this study are the following: to spatially and temporally quantify the contribution of the water evapotranspired from the Poyang Lake region to local precipitation, to precipitation in the Poyang Lake basin, and to precipitation in Southeast China using the RCM-based ET-Tagging algorithm and to investigate the relative contribution of direct evaporation and transpiration from the source area to the spatial and temporal distribution of the tagged precipitation.

As we are particularly interested in elaborating on the impact of the advance and retreat of the East Asian monsoon on the land-atmosphere interaction for the Poyang Lake region, we perform our analysis for the period of one entire year on a monthly scale (15 month simulations including 3 months spin-up period).

Table 1. Physical Schemes and Configuration of the MM5 Model as Used in This Study[a]

	Selected Schemes
Short-wave radiation	Dudhia [*Dudhia*, 1989]
Long-wave radiation	RRTM [*Mlawer et al.*, 1997]
Land surface	OSU-LSM [*Chen and Dudhia*, 2001]
Planetary boundary layer	MRF-PBL [*Hong and Pan*, 1996]
Microphysics	Mixed phase (Reisner 1) [*Reisner et al.*, 1998]
	Configuration
Simulation domain	Northeast: 121.8°E 33.7°N
	Southwest: 110.9°E 24.2°N
Domain size (grid points)	240 × 240
Horizontal resolution (km)	4.5
Time step (s)	10
Vertical discretization	33 Levels
σ levels	1.000, 0.996, 0.990, 0.983, 0.974, 0.963, 0.950, 0.934, 0.916, 0.896, 0.873, 0.848, 0.820, 0.789, 0.755, 0.718, 0.680, 0.640, 0.600, 0.560, 0.520, 0.480, 0.440, 0.400, 0.360, 0.320, 0.280, 0.240, 0.200, 0.160, 0.120, 0.080, 0.040, 0.000
Boundary update (h)	6
Output frequency	Hourly
Time period	3 months spin-up time (October–December 2004)
	12 months evaluation time (January–December 2005)

[a]MRF, Medium-Range Forecast.

In comparison with the source areas defined in other tagging studies [*Sodemann et al.*, 2009; *Wei et al.*, 2012a; *Winschall et al.*, 2014], our source area, i.e., the Poyang Lake region, is relatively small.

The structure of the article is as follows. Section 2 describes the basic RCM model used in this study, the ET-Tagging algorithm, and the ET-Tagging partitioning extension. Details of the ET-Tagging setup, including model configuration, source and target area specification, reference data, and evaluation strategy are explained in section 3. Section 4 hosts the results and a discussion of the application of the ET-Tagging and Partitioning algorithm over the Poyang Lake region in Southeast China. Section 4.1 presents the general performance of the RCM regarding precipitation and evapotranspiration in Southeast China. The distribution of the tagged moisture and tagged precipitation is shown in section 4.2. In section 4.3, an analysis of the atmospheric tagged water budget is presented, and the source-target relations corresponding to ET partitioning are explored in section 4.4. Finally, a summary is given and final conclusions are drawn in section 5.

2. Model and Methodology

The ET-Tagging and partitioning simulations were conducted with the Fifth-Generation Pennsylvania State University/National Center for Atmospheric Research Mesoscale Model (MM5) version 3.5 [*Dudhia*, 1993; *Grell et al.*, 1994]. MM5 is a process-based, nonhydrostatic model which simulates the behavior of a coupled dynamical system: atmosphere and soil, snow cover, and vegetation. The MM5 model has been applied extensively for short-period weather prediction and long-term climatological assessment at synoptic and subsynoptic scales. As a limited-area model, it allows for the representation of small-scale meteorological fields driven by external simulations (e.g., general circulation model simulations) or reanalysis data (e.g., ERA Interim).

MM5 uses a horizontal grid with an Arakawa-Lamb B grid staggering, based on a Lambert Conformal, Polar Stereographic, or Mercator map projection. In the vertical direction, a terrain-following sigma coordinate is used [*Dudhia*, 1993]. MM5 accounts for atmospheric diffusive and turbulent processes, short- and long-wave radiation, phase transitions of water substance, and the formation of precipitation. For each physical mechanism, a variety of different parameterizations and options are available. The schemes selected for this study are listed in section 3.1 and in Table 1.

2.1. ET-Tagging Algorithm

The MM5 model with the implemented ET-Tagging algorithm is used to explicitly quantify the contribution of land surface evapotranspiration to regional precipitation [*Knoche and Kunstmann*, 2013]. The concept of the ET-Tagging algorithm is to add a second numerical formulation of the atmospheric hydrological cycle to a RCM [*Sodemann et al.*, 2009; *Winschall et al.*, 2012; *Sodemann and Stohl*, 2013; *Winschall et al.*, 2014], i.e., the tagged moisture: evapotranspiring water from a selected region is "tagged" when entering the atmosphere. Then, the tagged moisture undergoes the same atmospheric processes as the (original) total moisture. Finally, the tagged moisture returns to the land surface as precipitation or leaves the model domain.

In our MM5 ET-Tagging environment, we define a mask over the whole model domain for separating a selected source area from its surroundings:

$$\mathrm{MASK}_{\mathrm{tag}} = \begin{cases} 1 & \text{for tagging source area} \\ 0 & \text{otherwise} \end{cases} \tag{1}$$

Upward ET fluxes (ET > 0) entering the lowest atmospheric model layer from the source area contribute to the tagged water vapor. Downward fluxes of tagged water vapor, i.e., dew formation, are also considered. The tagged downward fluxes $\mathrm{ET}_{\mathrm{tag}}$ (i.e., tagged dew formation) are proportional to the total downward fluxes ET (ET < 0) and the fraction of tagged water vapor $q_{v,\mathrm{tag}}^{\mathrm{lowest}}$ to total water vapor $q_{v,\mathrm{total}}^{\mathrm{lowest}}$ in the lowest model layer:

$$\mathrm{ET}_{\mathrm{tag}} = \begin{cases} \mathrm{ET} \cdot \mathrm{MASK}_{\mathrm{tag}} & \text{if } \mathrm{ET} \geq 0 \\ \mathrm{ET} \cdot q_{v,\mathrm{tag}}^{\mathrm{lowest}} / q_{v,\mathrm{total}}^{\mathrm{lowest}} & \text{if } \mathrm{ET} < 0 \end{cases} \tag{2}$$

For tracking the tagged water pathways through the atmosphere, the original MM5 moisture equations describing grid-scale transport, subgrid-scale transport due to turbulence and diffusion, phase transitions, and the downward transport of precipitating water components are duplicated in the code. The original equation set accounts for the total moisture components (here water vapor $q_{v,\mathrm{total}}$, cloud water $q_{c,\mathrm{total}}$, cloud ice $q_{i,\mathrm{total}}$, rain water $q_{r,\mathrm{total}}$, and snow $q_{s,\mathrm{total}}$), while the second equation set is for the tagged moisture components (i.e., $q_{v,\mathrm{tag}}$, $q_{c,\mathrm{tag}}$, $q_{i,\mathrm{tag}}$, $q_{r,\mathrm{tag}}$, and $q_{s,\mathrm{tag}}$). The ET fluxes at the land surface appear implicitly as boundary values for the atmospheric subgrid-scale fluxes. More details about the implementation of the ET-Tagging algorithm into the MM5 model are given in *Knoche and Kunstmann* [2013]. It should be noted that there is an alternative way of parameterizing tracer evapotranspiration using the moisture gradient of the individual tracers [e.g., *Sodemann et al.*, 2009]. Detailed comparisons and discussions of the two methods are given in *Winschall et al.* [2014] and *Goessling and Reick* [2013].

2.2. ET-Tagging Partitioning Extension

For the assessment of the contribution of the individual ET components on precipitation, additional model extensions concerning the partitioning of ET are introduced. The ET output of MM5 consists of evaporation from inland water bodies E_{water}, evaporation from the top shallow soil layer E_{soil}, evaporation of precipitation intercepted by the canopy $E_{\mathrm{interception}}$, and transpiration via canopy and roots by vegetation E_t:

$$\mathrm{ET} = \underbrace{E_{\mathrm{water}} + E_{\mathrm{soil}} + E_{\mathrm{interception}}}_{E_d} + E_t \tag{3}$$

E_{water} is governed by a Penman-based energy balance approach for potential evaporation. E_{soil} depends on soil moisture content and potential evaporation, and $E_{\mathrm{intercption}}$ is determined by the intercepted canopy water content and potential evaporation. E_t is calculated mainly by considering green vegetation fraction, potential evaporation, and soil moisture in the root zone. A detailed description of the land surface model is given in *Chen and Dudhia* [2001].

In this study, we extend the model to partition the evapotranspiration flux ET into a direct evaporation flux E_d (consisting of E_{water}, E_{soil}, and $E_{\mathrm{interception}}$) and a transpiration flux E_t and track the two fluxes separately.

To quantify the contribution of evapotranspiration to precipitation, a local precipitation contribution ratio ρ is defined as

$$\rho = P_{\mathrm{tag}} / P_{\mathrm{total}} \tag{4}$$

P_{tag} denotes the tagged precipitation contribution of ET from a predefined source area, while P_{total} denotes the total precipitation originating from local ET and remote moisture sources.

In the context of ET-Tagging partitioning (see equation (3)), we split the tagged evapotranspiration into tagged direct evaporation $E_{d,tag}$ and tagged transpiration $E_{t,tag}$

$$ET_{tag} = E_{d,tag} + E_{t,tag} \tag{5}$$

The tagged precipitation is split accordingly as

$$P_{tag} = P_{tag,E_d} + P_{tag,E_t} \tag{6}$$

3. ET-Tagging Study Design

3.1. Model Configuration

Preliminary model runs with different domain size, and grid spacing were performed for the identification of a suitable model setup. We concluded on a model domain covering Southeast China (see Figure 1a) with a horizontal resolution of 4.5 km and a vertical discretization of 33 layers up to 50 hPa with refined layers in the lower part of the atmosphere. The physical schemes applied in this study are the same as in *Knoche and Kunstmann* [2013] (see Table 1): We choose the revised Medium-Range Forecast model [*Hong and Pan*, 1996] to model the planetary boundary layer (PBL) and parameterize the turbulent processes. The cloud radiation short-wave scheme [*Dudhia*, 1989] and the Rapid Radiation Transfer Model (RRTM) long-wave scheme [*Mlawer et al.*, 1997] are selected for the calculation of the atmospheric short- and long-wave radiation. The Reisner-1 Mixed-Phase scheme [*Reisner et al.*, 1998] is used as the explicit microphysical parameterization, and the land surface model *Chen and Dudhia* [2001] is used with four vertical layers.

As mentioned by *Knoche and Kunstmann* [2013], with cumulus parametrization schemes, it is difficult to achieve a process-based treatment for moisture tagging modeling. Therefore, no cumulus parametrization is employed. This choice is extensively taken in many other studies [*Molinari and Dudek*, 1992; *Weisman et al.*, 1997; *Done et al.*, 2004; *Arakawa*, 2004; *Hong and Kim*, 2008; *Prein et al.*, 2013; *Lee et al.*, 2014]. The main reason is that at high resolution, the parameterisations are assumed to be obsolete because (deep) moist convection is (mostly) resolved at the grid scale. *Weisman et al.* [1997] states that approximately 4 km is usually sufficient to reproduce mesoscale systems. For this study, a model resolution of 4.5 km is chosen. This resolution is assumed to be fine enough to capture the convective systems sufficiently by grid-scale resolved dynamic model processes.

The global reanalysis data ERA Interim (with T255 spectral resolution $\approx$ 80 km and 60 vertical levels) [*Dee et al.*, 2011] from the European Centre for Medium-Range Weather Forecasts provides the initial and lateral boundary conditions. The hindcast simulation period covers 15 months from October 2004 to December 2005. The first 3 months are considered as model spin-up time, allowing the soil moisture and the tagged atmospheric moisture components to sufficiently develop. Regarding the spin-up time in our study, there are two considerations: for atmospheric fields, the spin-up time is rather short (i.e., 1 – 2 days) [*de Ela et al.*, 2002]. Hence, 2 weeks of simulation are generally enough to develop the tagged atmospheric moisture components [*Bosilovich and Schubert*, 2002]. In contrast, for some land surface processes (e.g., deep soil hydrology), the spin-up time is considerably longer [*Laprise*, 2008]: the long-term land surface interaction studies require several months of simulation to develop a consistent state of the soil moisture, for example, (up to 1 year in *Goessling and Reick* [2013]). In our previous work [*Knoche and Kunstmann*, 2013], 1 month is taken as a spin-up period for a rainy month of investigation. Thus, our choice of a 3 month spin-up time is a good compromise and sufficient for this investigation.

As the geographic source of tagged water, we defined an area of about 25,000 km^2 covering the Poyang Lake and its surrounding wetlands. This source area (hereafter referred to as area S) is shaded in red in Figure 1b. Figure 2 depicts the vegetation cover and land use types based on the global 25-category data from the U.S. Geological Survey (USGS) for area S. The area of the Poyang Lake (land use type 16) accounts for 13.5% of the total source area (Figure 2b). Irrigated crop (i.e., paddy rice) around the lake is the prime vegetation type with a fraction of 47.6% (land use type 3). Also depicted in Figure 1b are the model domain except a small

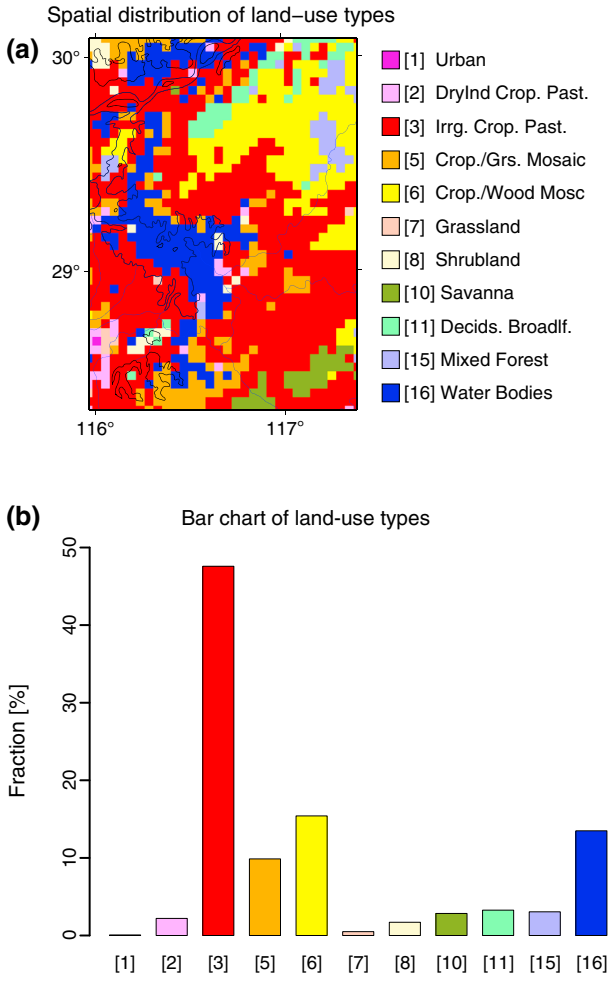

Figure 2. (a) Spatial distribution and (b) bar chart of the land use types for area S (horizontal resolution 4.5 km). The results are based on the global 25-category data from the U.S. Geological Survey (USGS).

boundary zone (area C, covering nearly all of Southeast China) and the Poyang Lake basin (area P). All these areas C, P, and S are considered as target areas in the analysis.

3.2. Reference Data and Evaluation Strategy

As reference data for precipitation, APHRODITE_V1003R1 (Asian Precipitation Highly Resolved Observational Data Integration Towards Evaluation of Water Resources) [*Yatagai et al.*, 2009, 2012] is used. The APHRODITE product provides long-term daily gridded precipitation data over Asia at 0.25°×0.25°resolution. It merges 2.3 to 4.5 times more rain gauge data compared to the data available through the Global Telecommunication System network [*Yatagai et al.*, 2009] and is assumed to better represent precipitation in complex terrain [*Yatagai et al.*, 2012].

As reference data for evapotranspiration, FLUXNET MTE (Model-Tree Ensemble), [*Jung et al.*, 2009, 2010, 2011] is used. The FLUXNET MTE product provides monthly gridded global evapotranspiration data at 0.5°×0.5°spatial resolution. It is derived by empirical upscaling of eddy covariance measurements from a global network of flux towers (FLUXNET) with a model tree ensemble (MTE) approach [*Jung et al.*, 2009].

For evaluation, the simulated precipitation and evapotranspiration were remapped to the respective reference data grids using a bilinear interpolation.

4. Results and Discussion

4.1. Simulated Precipitation and Evapotranspiration

Figure 3 depicts the total annual precipitation for 2005 from (a) APHRODITE and (b) our MM5 model simulation. Figures 3d and 3e show the total annual evapotranspiration for the same period from FLUXNET MTE and our simulation, respectively. Various smaller-scale structures are found in the simulation data, presumably due to the finer horizontal resolution of the original model output data. Generally, the MM5 model can reasonably reproduce the pattern of the reference data. Figures 3c and 3f show annual relative differences, which are larger near the domain boundary than in the center. The simulation tends to underestimate the total amount of precipitation, especially along the southeastern coast line and near the western boundary of the model domain. For evapotranspiration, the relative differences are small except in the regions in the northeast quadrant, where the land use type is inland water bodies. These deviations are partly attributed to the reference data: due to the weakness of the eddy covariance method used for FLUXNET MTE and the limited spatial representation [see *Jung et al.*, 2009, Figure 2], the evapotranspiration near distinct landscape transitions such as lakes is not well captured [*Baldocchi et al.*, 2001]. However, FLUXNET MTE is still the only territorial-based evapotranspiration data set on a long-term and continuous base. On the other hand, the MM5 model used in our study does not account for the impact of human activities, like for the irrigation of paddy rice. *Wei et al.* [2012b] found that irrigation-induced evapotranspiration caused only a small increase in precipitation, even in heavily irrigated central and northern China.

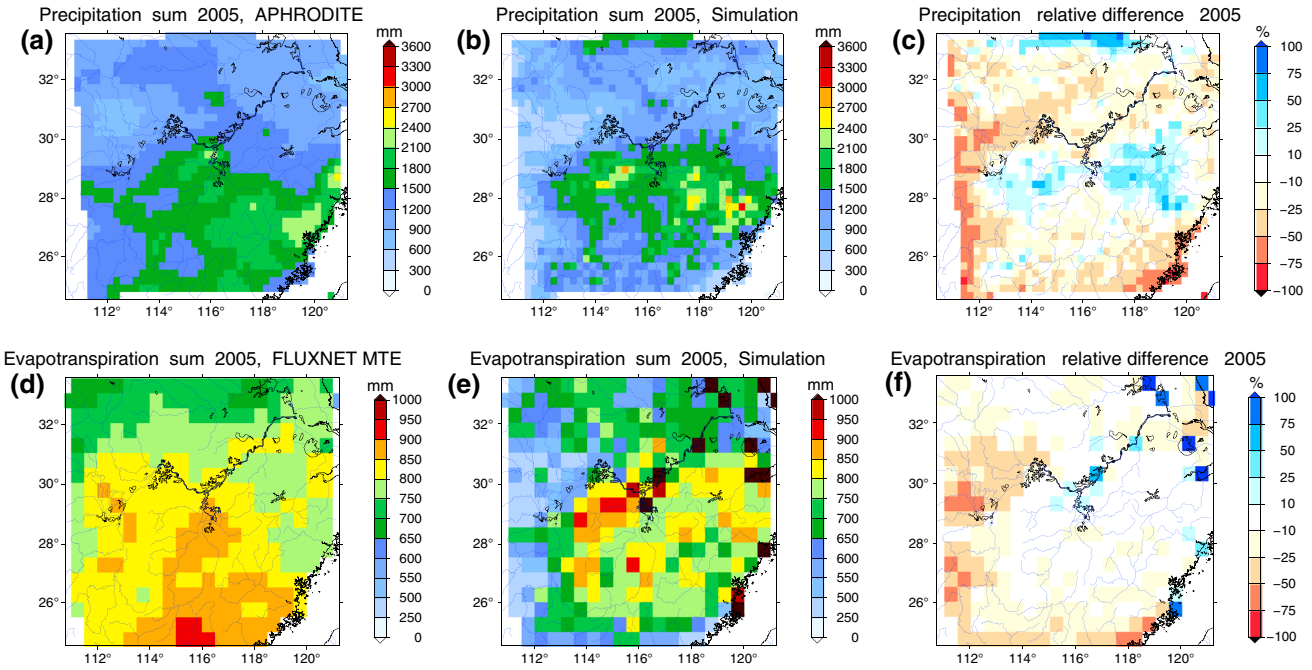

Figure 3. Annual total precipitation (mm) and evapotranspiration (mm) for Southeast China for 2005 from (a) APHRODITE and (d) FLUXNET MTE reference data, while our MM5 simulation interpolated (b) to the APHRODITE grid and (e) to the FLUXNET MTE grid. (c and f) The relative differences (%) between simulation and reference data.

Figure 4 shows the annual cycle of precipitation and evapotranspiration aggregated over the three analysis areas (see Figure 1b) for the year 2005. The model results show comparatively good agreement with the reference data. With the exception of May, where the simulated precipitation exceeds the observations in areas P and S, the model produces slightly too little rainfall. The annual cycle of the simulated evapotranspiration is also in good agreement with the reference data. Significantly, too small values are found only in summer, especially in August over the source area S. The reasons may be the slight underestimation of precipitation in

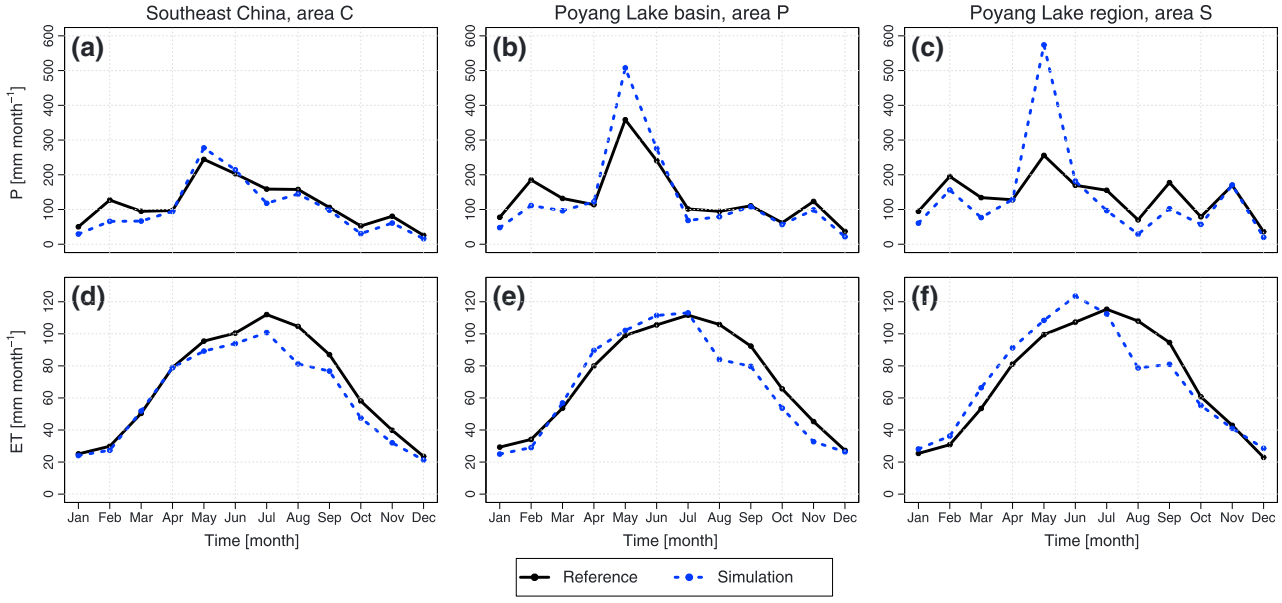

Figure 4. Comparison of simulation (dotted blue line) and reference data (solid black line). (a–c) Area-averaged, monthly time series of precipitation (mm month^{-1}) and (d–f) evapotranspiration (mm month^{-1}) for three evaluation regions (see Figure 1b): Figures 4a and 4d represent Southeast China, area C, Figures 4b and 4e represent Poyang Lake basin, area P, and Figures 4c and 4f represent Poyang Lake region, area S.

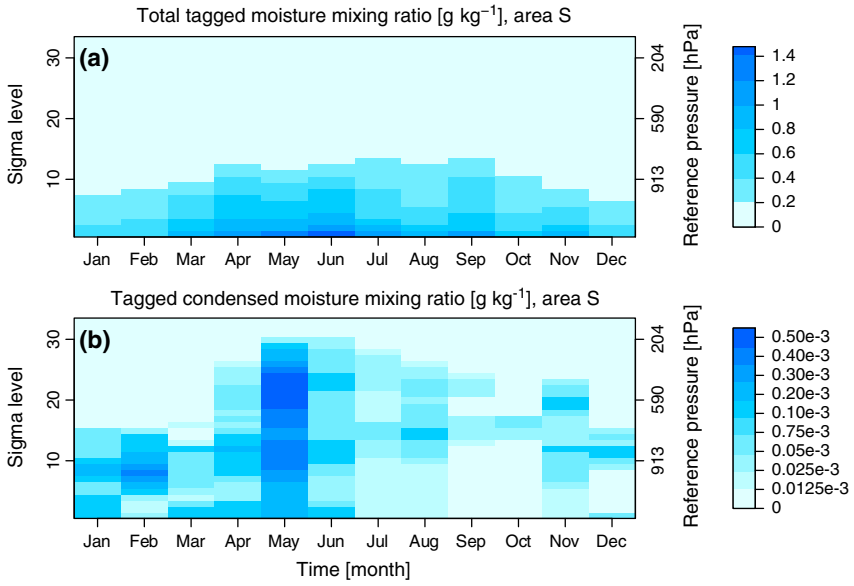

Figure 5. Monthly time series of vertical distribution of (a) total tagged moisture mixing ratio (g kg^{-1}) and (b) tagged condensed moisture mixing ratio (g kg^{-1}), averaged over area S for each model layer and for each month in 2005. The relative position of the sigma levels is given in Table 1.

this month and the neglection of irrigation schemes in our model. Nevertheless, our results indicate that the model also allows reasonable estimates of the tagged quantities.

4.2. Distribution of Tagged Moisture and Tagged Precipitation

The tagged moisture evapotranspired from the source area S is transported and spread in the atmosphere vertically and horizontally. Figure 5 shows the vertical distribution of (a) the total tagged moisture (consisting of water vapor, cloud water, cloud ice, rain water, and snow) and (b) the tagged condensed moisture (i.e., the sum of tagged liquid and solid cloud and precipitation water) over the source area S on monthly scales. Most of the tagged moisture remains in the boundary layer, with the maximum mixing ratio near the surface. The atmospheric storage of the tagged moisture increases from January to June and decreases from September to December and is associated with changes in the height of the boundary layer. In summer, high temperatures lead to enhanced evapotranspiration at the land surface, to an expansion of the boundary layer, and to an increased water storage capacity of the atmosphere.

The vertical distribution of the tagged *condensed* moisture is more diverse from month to month and is directly related to the formation of clouds and precipitation systems (see Figure 5b). As a result of more frequent convection and large-scale lifting, the tagged condensed moisture is found in higher atmospheric layers in the rainy season and in the summer season. For example, in May the main rain belt covers Southeast China, and the formation of convective clouds results in the tagged water vapor lifted up and condensed in the upper atmosphere above the planetary boundary layer. In contrast, in winter the tagged condensed moisture is predominantly formed in the lower atmospheric layers. Compared to the total tagged moisture, the tagged condensed moisture only accounts for a very small fraction.

To study the transport and distribution processes of tagged moisture from the source area, monthly vertical profiles of the three wind components averaged over the source area S are shown in Figure 6. It illustrates the variability of wind speed and wind direction with height and season. The direction of the meridional wind component changes in April and September due to the onset and retreat of the East Asian summer monsoon, respectively. The vertical wind component near the land surface switches from slightly downward to upward, during the summer monsoon season, with the strongest updraft in May, especially in the higher levels.

Figure 7a shows the horizontal distribution of the column-integrated total tagged moisture average for 2005. Generally, the horizontal distribution of the total tagged moisture is governed by the wind direction changes due to the development and retreat of the East Asian monsoon (see Figure 6) and influenced by the topography of the Poyang Lake basin (see Figure 1b). Most of the total tagged moisture is found above the Poyang

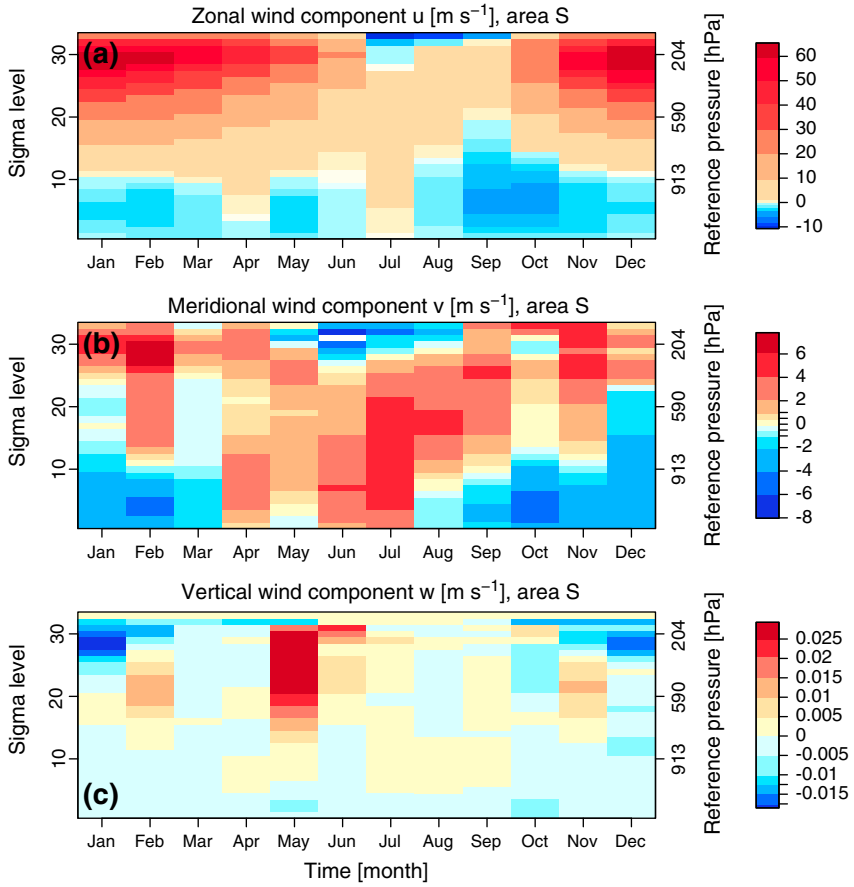

Figure 6. Monthly time series of vertical profile of wind components: (a) zonal velocity u (m s^{-1}), (b) meridional velocity v (m s^{-1}), and (c) vertical velocity w (m s^{-1}). The wind components are averaged over area S for each model layer and for each month in 2005.

Lake area (around 850 g m^{-2}) and directly west of it, due to the easterly wind prevailing most of the year in the boundary layer (see Figure 6a). With increasing distance from the source area, the total tagged moisture content distinctly declines.

Figure 7b depicts the horizontal distribution of the column-integrated *condensed* tagged moisture. Most of the condensed tagged moisture is contained in the atmosphere above the Poyang Lake region and in the adjacent part to the East and is, as suggested by Figure 5b, mainly formed during the rainy season. It indicates that the tagged moisture is involved in cloud formation and precipitating systems and is concentrated in the middle and high layers, where westerly winds dominate (see Figure 6b). The tagged condensed moisture found in the northern part of the domain results from the transportation processes by the prevailing southerly winds in summer. In contrast, the northerly winds in winter are responsible for the tagged condensed moisture appearing in the south.

Figure 8 shows the (a, d, g, and j) spatial distribution of the simulated total precipitation and (b, e, h, and k) tagged precipitation for 2005. The patterns of the local precipitation contribution ratio ρ (equation (4)) are also shown (Figures 8c, 8f, 8i, and 8l). In addition to the annual sum, 3 months (February, May, and August) are selected for illustrating the monthly variations of the tagged precipitation and its contribution patterns due to the advance and retreat of the East Asian monsoon.

Overall, the tagged precipitation patterns in Figure 8b are similar to the tagged condensed moisture patterns (see Figure 7b). Most of the tagged precipitation occurs around the source area S and in the adjacent part to the East with a maximum value of about 20 mm. In comparison to the total precipitation shown in Figure 8a, the tagged amount is nearly two orders of magnitude lower. Regions with maximum contribution ratio $\rho > 1.2$ % (the ratio of P_{tag} to P_{total}) in 2005 are found in the source area and in the north along the Yangtze River

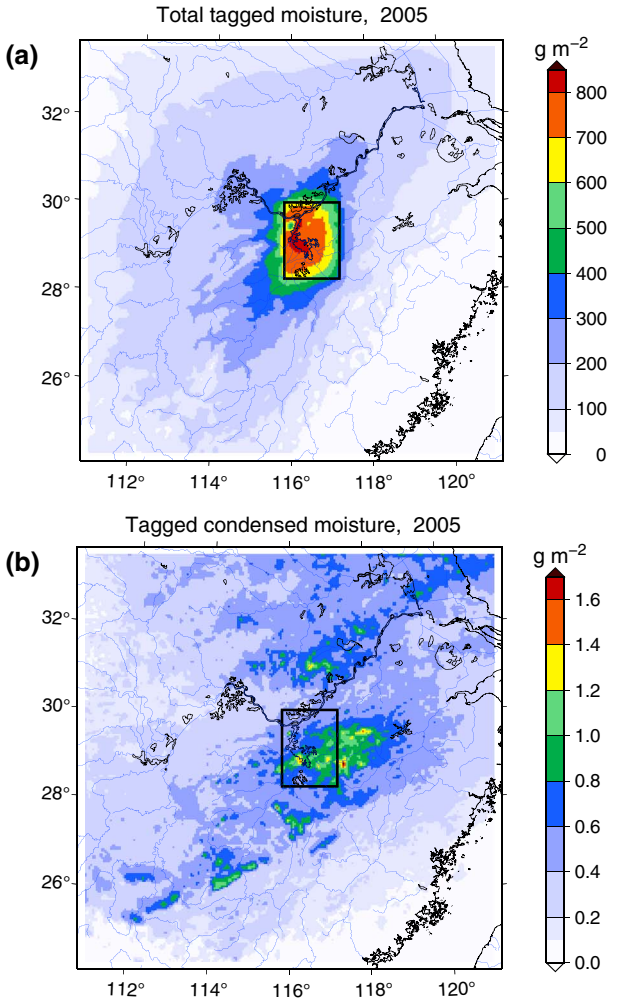

Figure 7. Horizontal distribution of (a) column-integrated total tagged moisture (g m^{-2}) and (b) column-integrated tagged condensed moisture (g m^{-2}), averaged for 2005. The color scale of Figures 7a and 7b ends at 850 g m^{-2} and 1.7 g m^{-2}, respectively.

Valley, about 200 km away from the Poyang Lake (Figure 8c). In contrast, the water evapotranspired from the Poyang Lake region does not significantly contribute to the precipitation in the southeast quadrant.

In February, the maximum values of tagged precipitation (only 1.2 mm) are found south of the source area (Figure 8e), where the dominant northerly winds are close to the land surface (see Figure 6). A smaller amount of tagged precipitation is also formed in the north because of the repeated changes in wind direction. The pattern of the contribution ratio of the monthly mean precipitation ρ in Figure 8f exhibits a band-like structure, shifted toward the south in the downwind regions. In the north, despite very low tagged precipitation sums, the contribution ratio reaches around 0.6 % due to equally low values of total precipitation. After the onset of the East Asian summer monsoon in April, the prevailing low-level and upper level winds rapidly reverse their directions. As discussed before, in May a large amount of tagged condensed moisture is locally involved in convective and large-scale precipitation processes. Therefore, the tagged precipitation amount reaches its maximum (15 mm) in the source area S and its surrounding regions (Figure 8h). The southerly winds also transport a small fraction of the tagged moisture toward the north, with some tagged precipitation occurring. Due to the low values of total precipitation (see Figure 8g), comparatively high contribution ratios are found in the north (Figure 8i). In August, due to the different wind directions near the land surface and in the upper level atmosphere, the tagged precipitation falls not only in the north but to a lesser extent also in the south (Figure 8k). Small fractions of tagged condensed moisture in higher model layers (see Figure 5b) lead to few local, convective rainfall events in and around the source area S, and to a contribution ratio of up to 6% near the eastern boundary of the source area S (Figure 8l), which is also the maximum on monthly scales for the year 2005. Our analysis of the selected 3 months reveals that the prevailing winds and the changing precipitation regime over Southeast China dominate the pattern of precipitation contribution. This finding is in general agreement with *van der Ent et al.* [2014].

4.3. Atmospheric Tagged Water Budget Analysis

To explore the relation between evapotranspiration from the source area and *tagged* precipitation in different geographic surrounding areas, an atmospheric tagged water budget analysis on monthly scales is performed. For this, the tagged evapotranspiration $ET_{tag,S}$ (mm $month^{-1}$) in the source area S is divided into five components:

$$ET_{tag,S} = P_{tag,S} + P_{tag,PoS} + P_{tag,CoPS} + \Delta Q_{tag,C} + F_{tag,C} \quad (7)$$

where $P_{tag,S}$, $P_{tag,PoS}$, and $P_{tag,CoPS}$ denote the tagged precipitation in area S, in area P but outside of S, and in area C but outside of P and S, respectively. $\Delta Q_{tag,C}$ is the storage change of the tagged moisture over

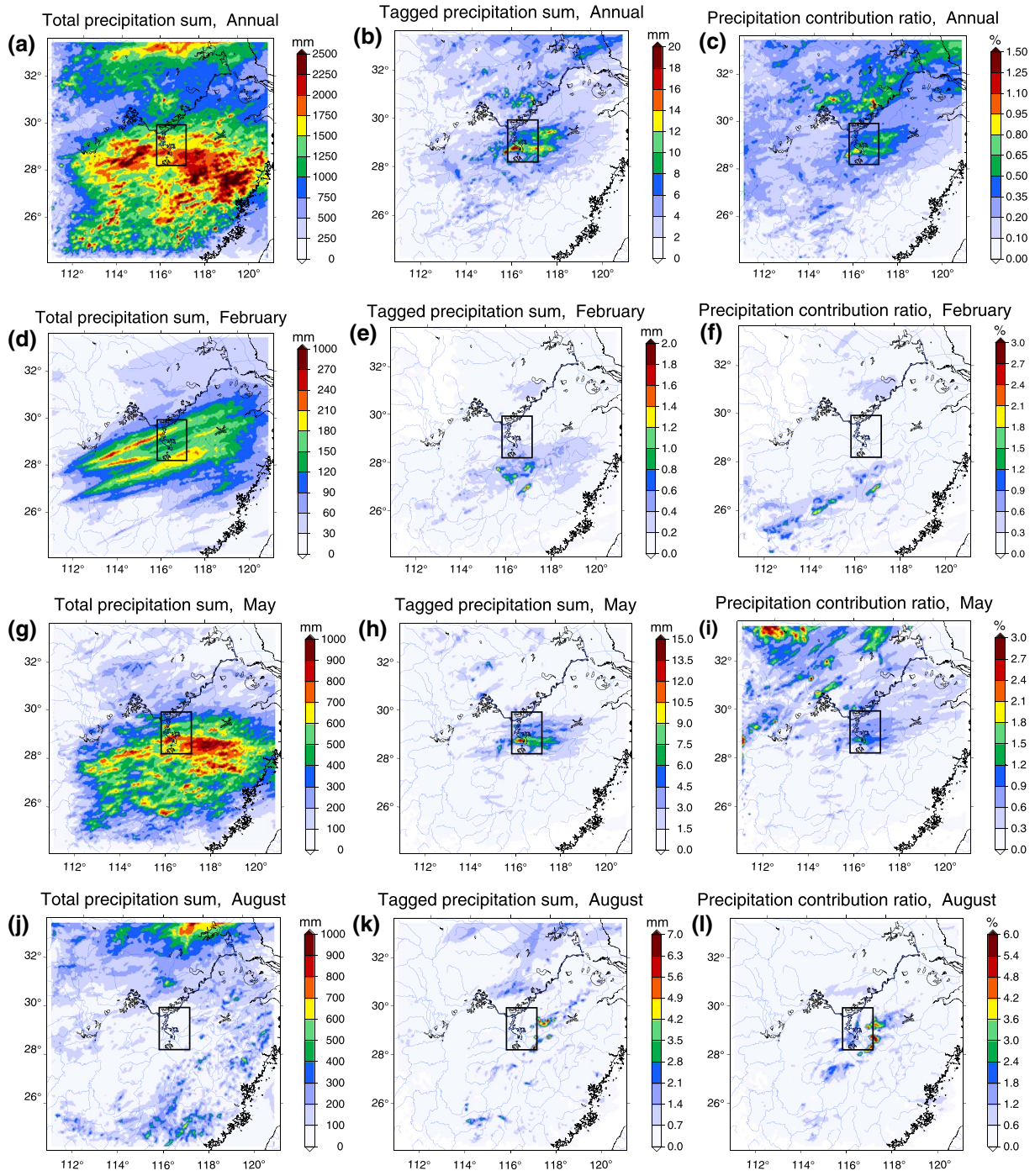

Figure 8. (a, d, g, and j) Annual sum and monthly sum of simulated total precipitation P_{total} in mm, (b, e, h, and k) tagged precipitation P_{tag} in mm, (c, f, i, and l), and (from top to bottom) annual/monthly mean of local precipitation contribution ρ in % for the whole year 2005 and 3 months (February, May, August).

area C, and $F_{tag,C}$ is the net lateral outflow flux of tagged moisture. $ET_{tag,S}$ and the tagged precipitation terms can be obtained directly from the ET-Tagging simulation. $\Delta Q_{tag,C}$ is calculated using the difference of the column-integrated total tagged moisture between the beginning and the end of a certain period, and $F_{tag,C}$ is determined as the residual in equation (7).

Table 2 summarizes the values of the tagged water budget terms on monthly scales for 2005. Overall, almost 90% of the evapotranspired tagged water leaves area C in 2005. Only 0.8% of the tagged moisture precipitates locally in the source area S with monthly values between 0.1% in October and 3.5% in May. In contrast,

Table 2. Atmospheric Tagged Water Budget (Equation (7)) of the ET-Tagging Simulation on Monthly Scales for 2005[a]

	$ET_{tag,S}$		$P_{tag,S}$		$P_{tag,PoS}$		$P_{tag,CoPS}$		$\Delta Q_{tag,C}$		$F_{tag,C}$		$P_{tag,P}$		$P_{tag,C}$	
Month	(%)	(mm)	(%)	(mm)	(%)	(mm)	(%)	(mm)	(%)	(mm)	(%)	(mm)	(%)	(mm)	(%)	(mm)
1	100.0	28.6	0.6	0.2	2.7	0.2	5.0	0.1	12.5	0.1	79.2	-	3.3	0.2	8.3	0.1
2	100.0	34.9	0.6	0.2	3.0	0.2	7.4	0.1	−0.2	0.0	89.2	-	3.5	0.2	11.0	0.1
3	100.0	66.0	0.2	0.1	1.4	0.2	5.3	0.1	3.4	0.1	89.7	-	1.6	0.2	6.9	0.1
4	100.0	94.4	0.6	0.6	1.4	0.3	7.2	0.2	−9.5	−0.2	100.3	-	2.0	0.3	9.2	0.2
5	100.0	106.0	3.5	3.8	5.9	1.3	15.3	0.5	12.5	0.4	62.8	-	9.2	1.7	24.7	0.7
6	100.0	125.0	0.6	0.7	1.2	0.3	8.6	0.3	−11.8	−0.4	101.4	-	1.7	0.4	10.4	0.3
7	100.0	123.0	0.3	0.4	0.6	0.1	7.6	0.3	5.3	0.2	86.2	-	0.8	0.2	8.5	0.3
8	100.0	87.8	0.4	0.3	2.2	0.4	11.5	0.3	2.5	0.1	83.4	-	2.6	0.4	14.2	0.3
9	100.0	86.9	0.2	0.2	1.4	0.3	6.0	0.2	4.1	0.1	88.3	-	1.6	0.2	7.6	0.2
10	100.0	60.5	0.1	0.1	0.8	0.1	2.2	0.0	−16.1	−0.3	113.0	-	0.9	0.1	3.1	0.1
11	100.0	41.7	1.2	0.5	2.3	0.2	5.8	0.1	15.8	0.2	74.9	-	3.5	0.3	9.3	0.1
12	100.0	31.0	0.2	0.1	1.4	0.1	2.9	0.0	−16.9	−0.1	112.4	-	1.6	0.1	4.5	0.0
Total	100.0	888.8	0.8	7.2	2.0	3.7	7.9	2.2	−0.1	0.0	89.4	-	2.7	4.3	10.7	2.5

[a]Monthly sums and changes during a month ($\Delta Q_{tag,C}$) are shown as relative values compared to $ET_{tag,S}$ in % and as precipitable water in mm. Source and target areas (see Figure 1b) are indicated as subscript for each term (S: the source area; P: the Poyang Lake basin; C: Southeast China; PoS: the area outside of S but inside of P; CoPS: the area outside of P and S but inside of C).

the comparison of $P_{tag,C}$ and $P_{tag,S}$ shows that due to the annual movement of the East Asian monsoon; the tagged precipitation is more often formed outside of the source area S. Averaged over 12 months, the tagged precipitation falling in the Poyang Lake basin (area P) equates to 2.7% of the tagged moisture with a maximum of 9.2% in May. Considering area C (representing nearly the whole of Southeast China), 10.7% of the tagged moisture returns as the tagged precipitation, with a maximum of 24.7% in May. The tagged precipitation contribution ratios in areas S, P, and C reveal the relevance of the evapotranspired water in the Poyang Lake region for tagged precipitation in Southeast China on different scales. Maximum values of tagged precipitation contribution ratios (i.e., significant recycling effects) are found in May when peak total (tagged and untagged) precipitation occurs.

In specific months like May and June but also from October to January, the wind regimes and the humidity of air masses over Southeast China change significantly. As a consequence, there are considerable differences in the atmospheric (tagged) moisture contents between the beginning and the end of the respective month. This explains the comparatively high values between −17% and +16% of the storage change term $\Delta Q_{tag,C}$.

4.4. Partitioning of Tagged Precipitation Corresponding to Partitioning of Evapotranspiration

According to equation (6), the tagged precipitation can be partitioned and is now separately analyzed. Figures 9a and 9b show the annual sum of P_{tag,E_d} and P_{tag,E_t} for 2005. Aggregated over area C, 69% of the tagged precipitation is contributed by direct evaporation and 31 % by transpiration. While higher values of P_{tag,E_d} are found in most parts of area C with a pronounced maximum over the source area S, higher values of P_{tag,E_t} are limited to the region around the source area and to (remote) northern areas. In these remote areas, large amounts of tagged transpired moisture in summer are transported by dominating southerly winds and subsequently contribute to precipitation. As a result, the distribution of the fraction $P_{tag,E_t}/P_{tag}$ in Figure 9c shows that the transpired water accounts for about half of the precipitation in the north. However, transpiration is far less important around the source area S and in the south ($P_{tag,E_t}/P_{tag} \leq 15\%$) due to the small contribution of tagged transpiration to total tagged evapotranspiration in winter.

Recently, *van der Ent et al.* [2014] found that in Southeast China, the continental precipitation recycling ratio for transpiration is larger than that for evaporation. This stands in contrast to our findings and is mainly ascribed to the different representations of land surface characteristics of the source areas in the two studies. The continent as a source area provides much more transpiration than direct evaporation. This means that transpiration dominates the terrestrial water cycle [*Jasechko et al.*, 2013; *Schlesinger and Jasechko*, 2014; *Wang-Erlandsson et al.*, 2014]. By contrast, our source area has a large fraction of moist land use types (water

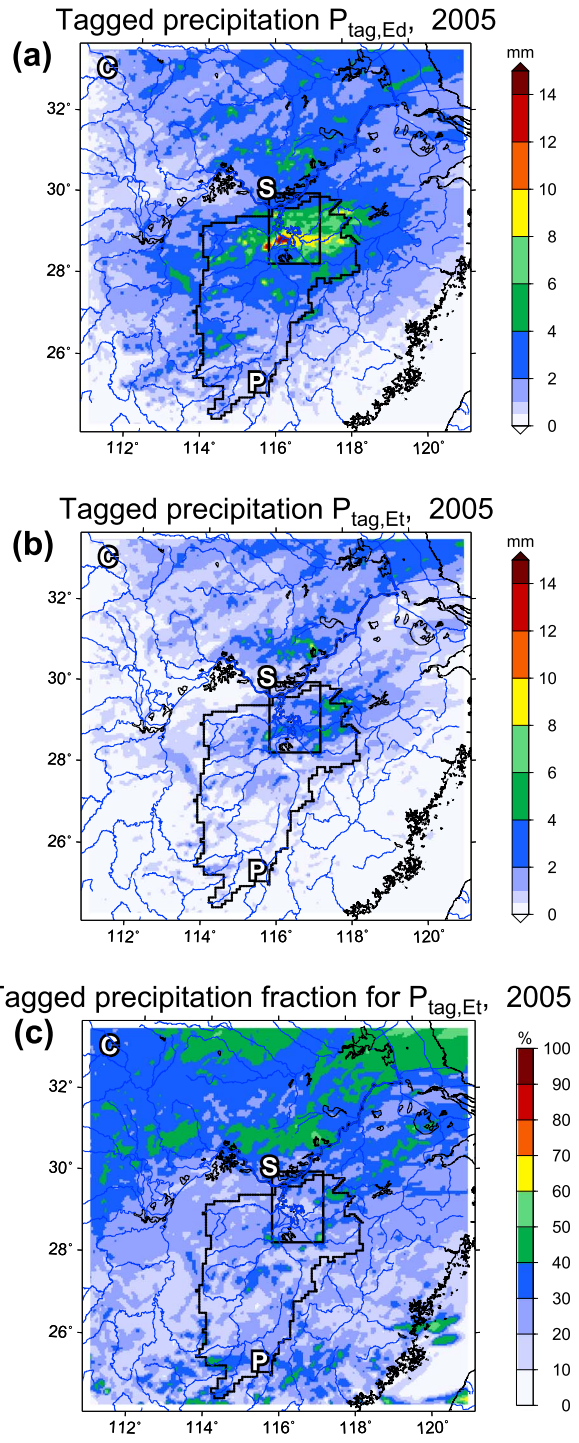

Figure 9. Annual sum of the simulated (a) tagged precipitation P_{tag,E_d} (mm) for direct evaporation and (b) tagged precipitation P_{tag,E_t} (mm) for transpiration and (c) annual mean of tagged precipitation fraction $P_{tag,E_t}/P_{tag}$ (%) for transpiration for the year 2005.

bodies and wetlands) with direct evaporation. This process is more effective for water at or near the surface than transpiration for water from the root zone [*Jasechko et al.*, 2013]. Overall, the different finding reveals that the vegetation cover and land use type have important impacts on the regional atmospheric hydrological cycle.

Next, we investigate the geographical distribution of evapotranspiration and tagged precipitation on a monthly basis. Figure 10a shows time series of monthly area mean of ET_{tag} and the corresponding partitioning over area S for 2005. Except for July, August, and September, the direct evaporation fluxes $E_{d,tag}$ show significantly higher values than the transpiration fluxes $E_{t,tag}$. They reach their maximum during the rainy season, since a large amount of water is available at the land surface. The monthly variation of the transpiration fraction $E_{t,tag}$ coincides with the seasonal changes in temperature. Since the land surface model in this study uses a prescribed seasonal varying climatological green leaf area index and green vegetation fraction, increasing temperatures reflect promoting transpiration and allow for more water uptake from the root zone. Thus, the highest values of $E_{t,tag}$ are found from June to September.

Correspondingly, time series of monthly area mean of the tagged precipitation P_{tag} and its fractions P_{tag,E_d} and P_{tag,E_t} over the source area S and over the target area C are shown in Figures 10b and 10c. In general, since little tagged precipitation for transpiration is found in winter and in the transit seasons, almost all of the tagged precipitation during these periods originates from direct evaporation. In the summer season, the transpiration becomes more important for the formation of tagged precipitation. For the small source area S, both P_{tag,E_d} and P_{tag,E_t} show the largest values in May (Figure 10b), in accordance with peak total (tagged and untagged) precipitation. For the large target area C, the time series of the tagged precipitation (Figure 10c) follows the trend of the source area S (see Figure 10b) but with less variation and markedly lower values in May, since P_{tag,E_t} is concentrated around the source area S due to frequent, local rainfall events. Relatively high values for P_{tag,E_t} persist from May to August.

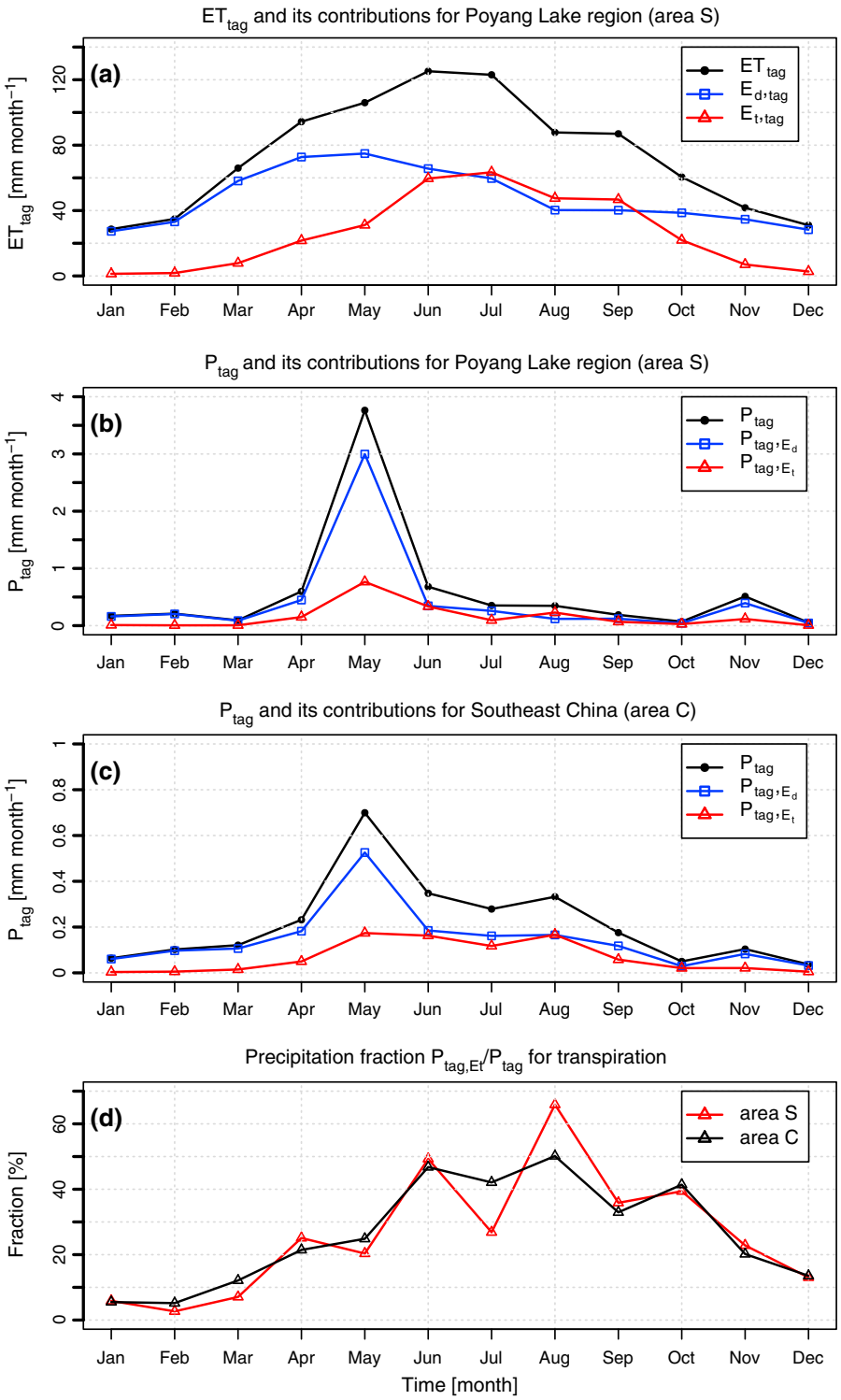

Figure 10. Time series of monthly area mean of (a) evapotranspiration ET_{tag} (black) and its contributions direct evaporation $E_{d,tag}$ (blue) and transpiration $E_{t,tag}$ (red) (mm month^{-1}) for area S, (b) tagged precipitation P_{tag} (black) and its contributions tagged precipitation for direct evaporation P_{tag,E_d} (blue) and for transpiration P_{tag,E_t} (red) (mm month^{-1}) for area S, (c) as in Figure 10b, except for area C, and (d) precipitation fraction $P_{tag,E_t}/P_{tag}$ for transpiration for area S (red) and for area C (black) (%).

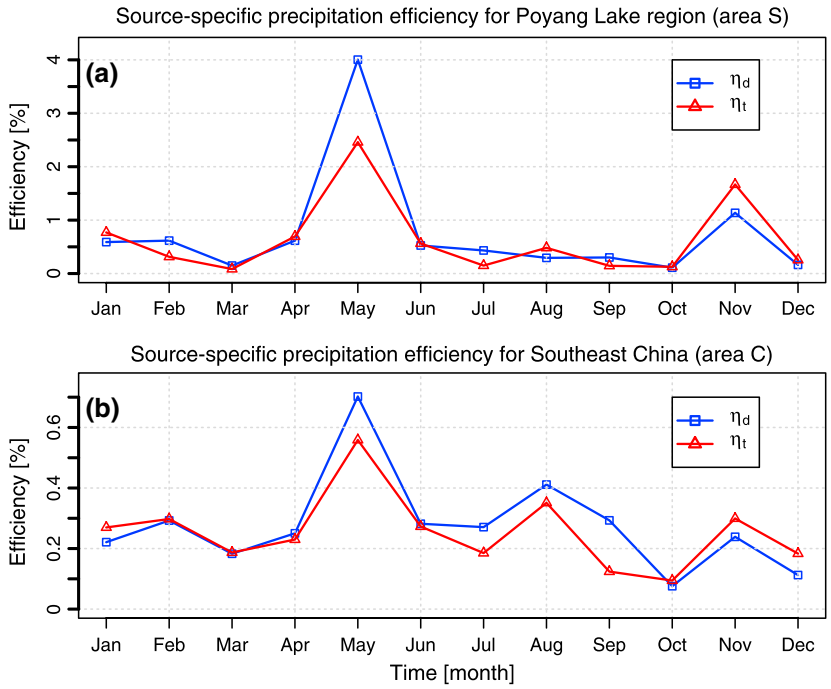

Figure 11. (a) Time series of monthly source-specific precipitation efficiency for direct evaporation η_d (%) in blue and for transpiration η_t (%) in red for area S, (b) as in Figure 11a, except for area C.

Additionally, time series of the ratio $P_{\text{tag},E_t}/P_{\text{tag}}$ for transpiration are given in Figure 10d. Larger fractions of $P_{\text{tag},E_t}/P_{\text{tag}}$ for the source area S are found in June and August with maximum ratios of around 50% and 66%. For area S, in May, due to the large amount of P_{tag,E_d} formed, P_{tag,E_t} only accounts for 25% of P_{tag}, while in the dry and warm season (from June to August), P_{tag,E_t} accounts for around 50% of P_{tag}.

The comparison of the monthly precipitation ratios over the source area S and over area C (see Figure 10d) reveals that in specific months, large fractions of direct evaporated moisture and of transpirated moisture are affected by different precipitation regimes. For example, in July, transpired water is transported over long distances and involved in remote rainfall events. In contrast, for example, local (area S) precipitation contribution by transpiration is more significant in August.

To explore further the source-target relations under consideration of the respective precipitation regime (wet or dry weather conditions), we introduce the source-specific precipitation efficiency

$$\eta = P_{\text{tag}}/\text{ET}_{\text{tag}}, \tag{8}$$

describing the relation of water that enters the domain from a specific source area by evapotranspriation and that subsequently falls as precipitation. In contrast to the precipitation efficiency defined in other studies [*Schär et al.*, 1999; *Kunstmann and Jung*, 2007], we focus on the evapotranspired water from a specific source area rather than from the whole domain or from outside. Similarly, in the context of ET-Tagging partitioning, the source-specific precipitation efficiency for direct evaporation is defined as

$$\eta_d = P_{\text{tag},E_d}/E_{d,\text{tag}} \tag{9}$$

and the source-specific precipitation efficiency for transpiration as

$$\eta_t = P_{\text{tag},E_t}/E_{t,\text{tag}}. \tag{10}$$

Figures 11a and 11b show the monthly values of the source-specific precipitation efficiencies η_d and η_t for the source area S and area C. The monthly variation of these parameters, which reflects different precipitation regimes, is closely connected to the monthly variation of the tagged precipitation and its fractions

(see Figures 10b and 10c). Generally, higher source-specific precipitation efficiencies imply a larger amount of precipitation being formed. As a result, the highest values of tagged precipitation are found in the rainy season in May, when the source-specific precipitation efficiencies also reach the highest values both for area S and for area C. For the small source area S, the source-specific precipitation efficiencies show a wider range of seasonal variation (Figure 11a). With the target area being larger (area C), the averaged source-specific precipitation efficiencies are lower and more uniform (Figure 11b).

5. Summary and Conclusions

A regional climate model with an ET-Tagging algorithm was applied to the Poyang Lake region (Southeast China) for 2005. This method, accounting for all water transport and phase transitions, follows the evapotranspired water pathways across the atmosphere until it precipitates in the model domain or leaves it. It was used to explicitly quantify the contribution of regional evapotranspiration to precipitation and to further evaluate the effect of land surface characteristics on hydrological processes by partitioning total evapotranspiration into direct evaporation and transpiration.

The study reveals that the location and magnitude of the tagged precipitation show large spatial and temporal variability controlled by synoptic weather conditions, especially by the wind shear due to the advance and retreat of the East Asian monsoon. Most tagged precipitation falls around the Poyang Lake region. In 2005, the tagged precipitation contribution accounts for up to 1.2% of the total rainfall. On a monthly scale, the maximum value of the contribution ratio is found in August ($\leq$ 6%). This relative low contribution of evapotranspiration from the Poyang Lake region to the precipitation in Southeast China means that the precipitation mainly originates from nonlocal moisture. This result is generally in line with previous studies by *Numaguti* [1999]; *Yoshimura et al.* [2004]; *van der Ent and Savenije* [2011]. In summer, nonlocal moisture contributions are mainly from the ocean, transported by the East Asian monsoon [*Wu et al.*, 2006], whereas in winter, it mainly comes from the north [*Chow et al.*, 2007]. Maximum values of tagged precipitation contribution ratios are consistently found in May, which reveals that the contribution of the Poyang Lake region becomes significant in accordance with peak total precipitation occuring.

Regarding the impact of vegetation cover and land use, in 2005 69% of the tagged precipitation in Southeast China is contributed by direct evaporation from the Poyang Lake region and 31% by vegetation transpiration. The annual cycle of these fractions reflects the changes of meteorological conditions and vegetation growth. In winter, the fraction of precipitation from transpiration accounts for only around 10% of the total tagged precipitation, while it reaches values of up to 50% for the remainder of the year.

Seasonal varying values of the source-specific precipitation efficiencies reveal a different response of the atmospheric hydrological cycle: warmer air temperature, increased convection, and large-scale lifting enhance the response of the atmospheric hydrological cycle to the direct evaporation from the Poyang Lake region, resulting in maximum values of the source-specific precipitation efficiencies in the rainy season. In May, the precipitation formation is more efficient for moisture originating from direct evaporation, while in the comparatively dry month August, the efficiency for transpiration dominates in the source area.

However, it is important to note that there are several limitations to the method used here: the results depend on how well physical processes like evapotranspiration, evapotranspiration partitioning, and precipitation are represented in the respective model system (here MM5). Moreover, this study did not account for the impact of human activities, like irrigation of paddy rice in the Poyang Lake region.

Our study is based on a 1 year simulation, because our focus is on the introduction and evaluation of methods to distinguish between direct evaporation and transpiration within the evapotranspiration tagging approach. We show that the partitioning has a clear intra-annual/seasonal variability in accordance with the general monsoon dynamics of the region and the vegetation response. Magnitudes of recycling and partitioning may defer from year to year but are expected to follow the monsoon controlled partitioning behavior. It is noted that for small tagging areas and accordingly small precipitation recycling ratios (like 1% mean in this study), uncertainties due to numerical approximations might have more influence on derived values than in cases of larger domains and larger precipitation recycling ratios.

In the future, our proposed high-resolution RCM-based evapotranspiration tagging and partitioning algorithm should be applied in sensitivity simulations and in further case studies to narrow down uncertainties. Although our study addresses only selected aspects of the complex relationships between land and

atmosphere, it emphasizes the important impacts of vegetation cover and land use on the regional atmospheric hydrological cycle. Our results depict the comprehensive interactions between land surface characteristics as simulated by a mesoscale model (e.g., water bodies, soil, and vegetation) and atmospheric variability such as the seasonal variation of the prevailing meteorological conditions. It is shown that there is a pronounced difference in the spatial range to which transpiration and evaporation are able to contribute to precipitation.

Acknowledgments
This work is funded by China Scholarship Council (CSC). The authors would like to thank the following data sources: European Centre for Medium-Range Weather Forecasts *ERA-Interim* (http://apps.ecmwf.int/datasets/), APHRODITE's Water Resources *APHRODITE* (http://www.chikyu.ac.jp/precip/), Max Plank Institute for Biogeochemistry *FLUXNET MTE* (http://www.bgc-jena.mpg.de/geodb/projects/Home.php). We thank Benjamin Fersch (KIT/IMK-IFU), Sven Wagner (KIT/IMK-IFU), Cornelia Klein (KIT/IMK-IFU), and Christof Lorenz (KIT/IMK-IFU) for their helpful technological supports and valuable scientific discussions. The help of Dominikus Heinzeller (KIT/IMK-IFU), Joël Arnault (KIT/IMK-IFU), and Patrick Laux (KIT/IMK-IFU) for proofreading the manuscript is gratefully acknowledged. We would like to thank two anonymous reviewers and Harald Sodemann for their detailed comments and suggestions that helped to improve our manuscript.

References

Arakawa, A. (2004), The cumulus parameterization problem: Past, present, and future, *J. Clim.*, *17*(13), 2493–2525, doi:10.1175/1520-0442(2004)017<2493:RATCPP>2.0.CO;2.

Bagley, J. E., A. R. Desai, P. A. Dirmeyer, and J. A. Foley (2012), Effects of land cover change on moisture availability and potential crop yield in the world's breadbaskets, *Environ. Res. Lett.*, *7*(1), 14,009, doi:10.1088/1748-9326/7/1/014009.

Baldocchi, D., et al. (2001), FLUXNET: A new tool to study the temporal and spatial variability of ecosystem-scale carbon dioxide, water vapor, and energy flux densities, *Bull. Am. Meteorol. Soc.*, *82*(11), 2415–2434, doi:10.1175/1520-0477(2001)082<2415:FANTTS>2.3.CO;2.

Bosilovich, M. G. (2002), On the vertical distribution of local and remote sources of water for precipitation, *Meteorol. Atmos. Phys.*, *80*(1–4), 31–41, doi:10.1007/s007030200012.

Bosilovich, M. G. (2003), Numerical simulation of the large-scale North American monsoon water sources, *J. Geophys. Res.*, *108*(D16), 8614, doi:10.1029/2002JD003095.

Bosilovich, M. G., and J.-D. Chern (2006), Simulation of water sources and precipitation recycling for the MacKenzie, Mississippi, and Amazon River Basins, *J. Hydrometeorol.*, *7*(3), 312–329, doi:10.1175/JHM501.1.

Bosilovich, M. G., and S. D. Schubert (2002), Water vapor tracers as diagnostics of the regional hydrologic cycle, *J. Hydrometeorol.*, *3*(2), 149–165, doi:10.1175/1525-7541(2002)003<0149:WVTADO>2.0.CO;2.

Bosilovich, M. G., S. D. Schubert, and G. K. Walker (2005), Global changes of the water cycle intensity, *J. Clim.*, *18*(10), 1591–1608, doi:10.1175/JCLI3357.1.

Burde, G. I., and A. Zangvil (2001), The estimation of regional precipitation recycling. Part I: Review of recycling models, *J. Clim.*, *14*(12), 2497–2508, doi:10.1175/1520-0442(2001)014<2497:TEORPR>2.0.CO;2.

Chen, F., and J. Dudhia (2001), Coupling an advanced land surface-hydrology model with the Penn State-NCAR MM5 modeling system. Part I: Model implementation and sensitivity, *Mon. Weather Rev.*, *129*(4), 569–585, doi:10.1175/1520-0493(2001)129<0569:CAALSH>2.0.CO;2.

Chow, K. C., H.-W. Tong, and J. C. L. Chan (2007), Water vapor sources associated with the early summer precipitation over China, *Clim. Dyn.*, *30*(5), 497–517, doi:10.1007/s00382-007-0301-6.

Dee, D. P., et al. (2011), The ERA-Interim reanalysis: Configuration and performance of the data assimilation system, *Q. J. R. Meteorol. Soc.*, *137*(656), 553–597, doi:10.1002/qj.828.

de Ela, R., R. Laprise, and B. Denis (2002), Forecasting skill limits of nested, limited-area models: A perfect-model approach, *Mon. Weather Rev.*, *130*(8), 2006–2023, doi:10.1175/1520-0493(2002)130<2006:FSLONL>2.0.CO;2.

Deng, X., Y. Zhao, F. Wu, Y. Lin, Q. Lu, and J. Dai (2011), Analysis of the trade-off between economic growth and the reduction of nitrogen and phosphorus emissions in the Poyang Lake watershed, China, *Ecol. Modell.*, *222*(2), 330–336, doi:10.1016/j.ecolmodel.2010.08.032.

Done, J., C. A. Davis, and M. Weisman (2004), The next generation of NWP: Explicit forecasts of convection using the Weather Research And Forecasting (WRF) model, *Atmos. Sci. Lett.*, *5*(6), 110–117, doi:10.1002/asl.72.

Druyan, L. M., and R. D. Koster (1989), Sources of Sahel precipitation for simulated drought and rainy seasons, *J. Clim.*, *2*(12), 1438–1446, doi:10.1175/1520-0442(1989)002<1438:SOSPFS>2.0.CO;2.

Dudhia, J. (1989), Numerical study of convection observed during the winter monsoon experiment using a mesoscale two-dimensional model, *J. Atmos. Sci.*, *46*(20), 3077–3107, doi:10.1175/1520-0469(1989)046<3077:NSOCOD>2.0.CO;2.

Dudhia, J. (1993), A nonhydrostatic version of the Penn State-NCAR mesoscale model: Validation tests and simulation of an Atlantic cyclone and cold front, *Mon. Weather Rev.*, *121*(5), 1493–1513, doi:10.1175/1520-0493(1993)121<1493:ANVOTP>2.0.CO;2.

Eltahir, E. A. B., and R. L. Bras (1996), Precipitation recycling, *Rev. Geophys.*, *34*(3), 367–378, doi:10.1029/96RG01927.

Gao, B., D. Yang, and H. Yang (2013), Impact of the Three Gorges Dam on flow regime in the middle and lower Yangtze River, *Quat. Int.*, *304*, 43–50, doi:10.1016/j.quaint.2012.11.023.

Gimeno, L., A. Stohl, R. M. Trigo, F. Dominguez, K. Yoshimura, L. Yu, A. Drumond, A. M. Durán-Quesada, and R. Nieto (2012), Oceanic and terrestrial sources of continental precipitation, *Rev. Geophys.*, *50*, RG4003, doi:10.1029/2012RG000389.

Goessling, H. F., and C. H. Reick (2011), What do moisture recycling estimates tell us? Exploring the extreme case of non-evaporating continents, *Hydrol. Earth Syst. Sci.*, *15*(10), 3217–3235, doi:10.5194/hess-15-3217-2011.

Goessling, H. F., and C. H. Reick (2013), On the "well-mixed" assumption and numerical 2-D tracing of atmospheric moisture, *Atmos. Chem. Phys.*, *13*(11), 5567–5585, doi:10.5194/acp-13-5567-2013.

Grell, A. G., J. Dudhia, and R. D. Stauffer (1994), A description of the fifth-generation Penn State/NCAR Mesoscale Model (MM5), *Tech. Rep. NCAR Tech. Note NCAR/TN-398+STR*,Mesoscale and Microscale Meteorology Division, National Center for Atmospheric Research, Pennsylvania State Univ., doi:10.5065/D60Z716B.

Hong, J., and J. Kim (2008), Scale-dependency of surface fluxes in an atmospheric mesoscale model: Effect of spatial heterogeneity in atmospheric conditions, *Nonlinear Process. Geophys.*, *15*(6), 965–975, doi:10.5194/npg-15-965-2008.

Hong, S.-Y., and H.-L. Pan (1996), Nonlocal boundary layer vertical diffusion in a medium-range forecast model, *Mon. Weather Rev.*, *124*(10), 2322–2339, doi:10.1175/1520-0493(1996)124<2322:NBLVDI>2.0.CO;2.

Huntington, T. G. (2006), Evidence for intensification of the global water cycle: Review and synthesis, *J. Hydrol.*, *319*(1–4), 83–95, doi:10.1016/j.jhydrol.2005.07.003.

Jacobs, C. M. J., and H. A. R. De Bruin (1992), The sensitivity of regional transpiration to land-surface characteristics: Significance of feedback, *J. Clim.*, *5*(7), 683–698, doi:10.1175/1520-0442(1992)005<0683:TSORTT>2.0.CO;2.

Jasechko, S., Z. D. Sharp, J. J. Gibson, S. J. Birks, Y. Yi, and P. J. Fawcett (2013), Terrestrial water fluxes dominated by transpiration, *Nature*, *496*(7445), 347–350, doi:10.1038/nature11983.

Jiao, L. (2009), Scientists line up against dam that would alter protected wetlands, *Science*, *326*(5952), 508–509, doi:10.1126/science.326_508.

Joussaume, S., R. Sadourny, and C. Vignal (1986), Origin of precipitating water in a numerical simulation of the July climate, *Ocean-Air Interact.*, *1*, 43–56.

Jung, M., M. Reichstein, and A. Bondeau (2009), Towards global empirical upscaling of FLUXNET eddy covariance observations: Validation of a model tree ensemble approach using a biosphere model, *Biogeosciences*, *6*(10), 2001–2013, doi:10.5194/bg-6-2001-2009.

Jung, M., et al. (2010), Recent decline in the global land evapotranspiration trend due to limited moisture supply, *Nature*, *467*(7318), 951–954, doi:10.1038/nature09396.

Jung, M., et al. (2011), Global patterns of land-atmosphere fluxes of carbon dioxide, latent heat, and sensible heat derived from eddy covariance, satellite, and meteorological observations, *J. Geophys. Res.*, *116*, G00J07, doi:10.1029/2010JG001566.

Karl, T. R., and K. E. Trenberth (2003), Modern global climate change, *Science*, *302*(5651), 1719–1723, doi:10.1126/science.1090228.

Keys, P. W., R. J. van der Ent, L. J. Gordon, H. Hoff, R. Nikoli, and H. H. G. Savenije (2012), Analyzing precipitationsheds to understand the vulnerability of rainfall dependent regions, *Biogeosciences*, *9*(2), 733–746, doi:10.5194/bg-9-733-2012.

Keys, P. W., E. A. Barnes, R. J. van der Ent, and L. J. Gordon (2014), Variability of moisture recycling using a precipitationshed framework, *Hydrol. Earth Syst. Sci.*, *18*(10), 3937–3950, doi:10.5194/hess-18-3937-2014.

Knoche, H. R., and H. Kunstmann (2013), Tracking atmospheric water pathways by direct evaporation tagging: A case study for West Africa, *J. Geophys. Res. Atmos.*, *118*, 12,345–12,358, doi:10.1002/2013JD019976.

Koster, R., J. Jouzel, R. Suozzo, G. Russell, W. Broecker, D. Rind, and P. Eagleson (1986), Global sources of local precipitation as determined by the Nasa/Giss GCM, *Geophys. Res. Lett.*, *13*(2), 121–124, doi:10.1029/GL013i002p00121.

Kunstmann, H., and G. Jung (2007), Influence of soil-moisture and land use change on precipitation in the Volta Basin of West Africa, *Int. J. River Basin Manag.*, *5*(1), 9–16, doi:10.1080/15715124.2007.9635301.

Lai, X., J. Jiang, G. Yang, and X. X. Lu (2014), Should the Three Gorges Dam be blamed for the extremely low water levels in the middle-lower Yangtze River?, *Hydrol. Process.*, *28*(1), 150–160, doi:10.1002/hyp.10077.

Laprise, R. (2008), Regional climate modelling, *J. Comput. Phys.*, *227*(7), 3641–3666, doi:10.1016/j.jcp.2006.10.024.

Lawrence, D. M., P. E. Thornton, K. W. Oleson, and G. B. Bonan (2007), The partitioning of evapotranspiration into transpiration, soil evaporation, and canopy evaporation in a GCM: Impacts on land-atmosphere interaction, *J. Hydrometeorol.*, *8*(4), 862–880, doi:10.1175/JHM596.1.

Lee, J., H. H. Shin, S.-Y. Hong, P. A. Jiménez, J. Dudhia, and J. Hong (2014), Impacts of sub-grid-scale orography parameterization on simulated surface-layer wind and monsoonal precipitation in the high-resolution WRF model, *J. Geophys. Res. Atmos.*, *120*, 644–653, doi:10.1002/2014JD022747.

Liu, B., M. Xu, M. Henderson, and Q. Ye (2005), Observed trends of precipitation amount, frequency, and intensity in China, 1960-2000, *J. Geophys. Res.*, *110*, D08103, doi:10.1029/2004JD004864.

Liu, Y., G. Wu, and X. Zhao (2013), Recent declines in China's largest freshwater lake: Trend or regime shift?, *Environ. Res. Lett.*, *8*(1), 14,010, doi:10.1088/1748-9326/8/1/014010.

Lo, M.-H., and J. S. Famiglietti (2013), Irrigation in California's Central Valley strengthens the southwestern U.S. water cycle, *Geophys. Res. Lett.*, *40*, 301–306, doi:10.1002/grl.50108.

Mlawer, E. J., S. J. Taubman, P. D. Brown, M. J. Iacono, and S. A. Clough (1997), Radiative transfer for inhomogeneous atmospheres: RRTM, a validated correlated-k model for the longwave, *J. Geophys. Res.*, *102*(D14), 16,663–16,682, doi:10.1029/97JD00237.

Molinari, J., and M. Dudek (1992), Parameterization of convective precipitation in mesoscale numerical models: A critical review, *Mon. Weather Rev.*, *120*(2), 326–344, doi:10.1175/1520-0493(1992)120<0326:POCPIM>2.0.CO;2.

Numaguti, A. (1999), Origin and recycling processes of precipitating water over the Eurasian continent: Experiments using an atmospheric general circulation model, *J. Geophys. Res.*, *104*(D2), 1957–1972, doi:10.1029/1998JD200026.

Prein, A. F., A. Gobiet, M. Suklitsch, H. Truhetz, N. K. Awan, K. Keuler, and G. Georgievski (2013), Added value of convection permitting seasonal simulations, *Clim. Dyn.*, *41*(9–10), 2655–2677, doi:10.1007/s00382-013-1744-6.

Reisner, J., R. M. Rasmussen, and R. T. Bruintjes (1998), Explicit forecasting of supercooled liquid water in winter storms using the MM5 mesoscale model, *Q. J. R. Meteorol. Soc.*, *124*(548), 1071–1107, doi:10.1002/qj.49712454804.

Rienecker, M. M., et al. (2011), MERRA: NASA's modern-era retrospective analysis for research and applications, *J. Clim.*, *24*(14), 3624–3648, doi:10.1175/JCLI-D-11-00015.1.

Schär, C., D. Lüthi, U. Beyerle, and E. Heise (1999), The soil-precipitation feedback: A process study with a regional climate model, *J. Clim.*, *12*(3), 722–741, doi:10.1175/1520-0442(1999)012<0722:TSPFAP>2.0.CO;2.

Schlesinger, W. H., and S. Jasechko (2014), Transpiration in the global water cycle, *Agric. Forest Meteorol.*, *189-190*, 115–117, doi:10.1016/j.agrformet.2014.01.011.

Seneviratne, S. I., D. Lüthi, M. Litschi, and C. Schär (2006), Land-atmosphere coupling and climate change in Europe, *Nature*, *443*(7108), 205–209, doi:10.1038/nature05095.

Seneviratne, S. I., T. Corti, E. L. Davin, M. Hirschi, E. B. Jaeger, I. Lehner, B. Orlowsky, and A. J. Teuling (2010), Investigating soil moisture-climate interactions in a changing climate: A review, *Earth Sci. Rev.*, *99*(3–4), 125–161, doi:10.1016/j.earscirev.2010.02.004.

Sewall, J. O., L. C. Sloan, M. Huber, and S. Wing (2000), Climate sensitivity to changes in land surface characteristics, *Global Planet. Change*, *26*(4), 445–465, doi:10.1016/S0921-8181(00)00056-4.

Shankman, D., B. D. Keim, and J. Song (2006), Flood frequency in China's Poyang Lake region: Trends and teleconnections, *Int. J. Climatol.*, *26*(9), 1255–1266, doi:10.1002/joc.1307.

Shankman, D., B. D. Keim, T. Nakayama, R. Li, D. Wu, and W. C. Remington (2012), Hydroclimate analysis of severe floods in China's Poyang Lake region, *Earth Interact.*, *16*(14), 1–16, doi:10.1175/2012EI000455.1.

Simmonds, I., D. Bi, and P. Hope (1999), Atmospheric water vapor flux and its association with rainfall over China in summer, *J. Clim.*, *12*(5), 1353–1367, doi:10.1175/1520-0442(1999)012<1353:AWVFAI>2.0.CO;2.

Sodemann, H., and A. Stohl (2013), Moisture origin and meridional transport in atmospheric rivers and their association with multiple cyclones*, *Mon. Weather Rev.*, *141*(8), 2850–2868, doi:10.1175/MWR-D-12-00256.1.

Sodemann, H., H. Wernli, and C. Schwierz (2009), Sources of water vapour contributing to the Elbe flood in August 2002—A tagging study in a mesoscale model, *Q. J. R. Meteorol. Soc.*, *135*(638), 205–223, doi:10.1002/qj.374.

Trenberth, K. E. (1998), Atmospheric moisture residence times and cycling: Implications for rainfall rates and climate change, *Clim. Change*, *39*(4), 667–694, doi:10.1023/A:1005319109110.

Trenberth, K. E. (1999), Atmospheric moisture recycling: Role of advection and local evaporation, *J. Clim.*, *12*(5), 1368–1381, doi:10.1175/1520-0442(1999)012<1368:AMRROA>2.0.CO;2.

Trenberth, K. E., and C. J. Guillemot (1995), Evaluation of the global atmospheric moisture budget as seen from analyses, *J. Clim.*, *8*(9), 2255–2272, doi:10.1175/1520-0442(1995)008<2255:EOTGAM>2.0.CO;2.

Tuinenburg, O. A., R. W. A. Hutjes, and P. Kabat (2012), The fate of evaporated water from the Ganges basin, *J. Geophys. Res.*, *117*, D01107, doi:10.1029/2011JD016221.
van der Ent, R. J., and H. H. G. Savenije (2011), Length and time scales of atmospheric moisture recycling, *Atmos. Chem. Phys.*, *11*(5), 1853–1863, doi:10.5194/acp-11-1853-2011.
van der Ent, R. J., and H. H. G. Savenije (2013), Oceanic sources of continental precipitation and the correlation with sea surface temperature, *Water Resour. Res.*, *49*, 3993–4004, doi:10.1002/wrcr.20296.
van der Ent, R. J., H. H. G. Savenije, B. Schaefli, and S. C. Steele-Dunne (2010), Origin and fate of atmospheric moisture over continents, *Water Resour. Res.*, *46*, W09525, doi:10.1029/2010WR009127.
van der Ent, R. J., O. A. Tuinenburg, H.-R. Knoche, H. Kunstmann, and H. H. G. Savenije (2013), Should we use a simple or complex model for moisture recycling and atmospheric moisture tracking?, *Hydrol. Earth Syst. Sci.*, *17*(12), 4869–4884, doi:10.5194/hess-17-4869-2013.
van der Ent, R. J., L. Wang-Erlandsson, P. W. Keys, and H. H. G. Savenije (2014), Contrasting roles of interception and transpiration in the hydrological cycle—Part 2: Moisture recycling, *Earth Syst. Dyn.*, *5*(2), 471–489, doi:10.5194/esd-5-471-2014.
Wang, K., and R. E. Dickinson (2012), A review of global terrestrial evapotranspiration: Observation, modeling, climatology, and climatic variability, *Rev. Geophys.*, *50*, RG2005, doi:10.1029/2011RG000373.
Wang-Erlandsson, L., R. J. van der Ent, L. J. Gordon, and H. H. G. Savenije (2014), Contrasting roles of interception and transpiration in the hydrological cycle—Part 1: Temporal characteristics over land, *Earth Syst. Dyn.*, *5*(2), 441–469, doi:10.5194/esd-5-441-2014.
Wei, J., P. A. Dirmeyer, M. G. Bosilovich, and R. Wu (2012a), Water vapor sources for Yangtze River Valley rainfall: Climatology, variability, and implications for rainfall forecasting, *J. Geophys. Res.*, *117*, D05126, doi:10.1029/2011JD016902.
Wei, J., P. A. Dirmeyer, D. Wisser, M. G. Bosilovich, and D. M. Mocko (2012b), Where does the irrigation water go? An estimate of the contribution of irrigation to precipitation using MERRA, *J. Hydrometeorol.*, *14*(1), 275–289, doi:10.1175/JHM-D-12-079.1.
Weisman, M. L., W. C. Skamarock, and J. B. Klemp (1997), The resolution dependence of explicitly modeled convective systems, *Mon. Weather Rev.*, *125*(4), 527–548, doi:10.1175/1520-0493(1997)125<0527:TRDOEM>2.0.CO;2.
Winschall, A., S. Pfahl, H. Sodemann, and H. Wernli (2012), Impact of North Atlantic evaporation hot spots on southern Alpine heavy precipitation events, *Q. J. R. Meteorol. Soc.*, *138*(666), 1245–1258, doi:10.1002/qj.987.
Winschall, A., S. Pfahl, H. Sodemann, and H. Wernli (2014), Comparison of Eulerian and Lagrangian moisture source diagnostics—The flood event in eastern Europe in May 2010, *Atmos. Chem. Phys.*, *14*(13), 6605–6619, doi:10.5194/acp-14-6605-2014.
Wu, S., Y. Yin, D. Zheng, and Q. Yang (2006), Moisture conditions and climate trends in China during the period 1971–2000, *Int. J. Climatol.*, *26*(2), 193–206, doi:10.1002/joc.1245.
Xie, H., P. Wang, and H. Huang (2013), Ecological risk assessment of land use change in the Poyang Lake eco-economic zone, China, *Int. J. Environ. Res. Public Health*, *10*(1), 328–346, doi:10.3390/ijerph10010328.
Yatagai, A., O. Arakawa, K. Kamiguchi, H. Kawamoto, M. I. Nodzu, and A. Hamada (2009), A 44-year daily gridded precipitation dataset for Asia based on a dense network of rain gauges, *SOLA*, *5*, 137–140, doi:10.2151/sola.2009-035.
Yatagai, A., K. Kamiguchi, O. Arakawa, A. Hamada, N. Yasutomi, and A. Kitoh (2012), APHRODITE: Constructing a long-term daily gridded precipitation dataset for Asia based on a dense network of rain gauges, *Bull. Am. Meteorol. Soc.*, *93*(9), 1401–1415, doi:10.1175/BAMS-D-11-00122.1.
Ye, X., Q. Zhang, L. Bai, and Q. Hu (2011), A modeling study of catchment discharge to Poyang Lake under future climate in China, *Quat. Int.*, *244*(2), 221–229, doi:10.1016/j.quaint.2010.07.004.
Ye, X., Q. Zhang, J. Liu, X. Li, and C.-y. Xu (2013), Distinguishing the relative impacts of climate change and human activities on variation of streamflow in the Poyang Lake catchment, China, *J. Hydrol.*, *494*, 83–95, doi:10.1016/j.jhydrol.2013.04.036.
Yoshimura, K., T. Oki, N. Ohte, and S. Kanae (2004), Colored moisture analysis estimates of variations in 1998 Asian monsoon water sources, *J. Meteorol. Soc. Jpn.*, *82*(5), 1315–1329, doi:10.2151/jmsj.2004.1315.
Zhang, Q., C.-Y. Xu, Z. Zhang, Y. D. Chen, C.-l. Liu, and H. Lin (2008), Spatial and temporal variability of precipitation maxima during 1960–2005 in the Yangtze River basin and possible association with large-scale circulation, *J. Hydrol.*, *353*(3–4), 215–227, doi:10.1016/j.jhydrol.2007.11.023.
Zhang, Q., Y. Liu, G. Yang, and Z. Zhang (2011), Precipitation and hydrological variations and related associations with large-scale circulation in the Poyang Lake basin, China, *Hydrol. Process.*, *25*(5), 740–751, doi:10.1002/hyp.7863.
Zhang, Q., L. Li, Y.-G. Wang, A. D.Werner, P. Xin, T. Jiang, and D. A. Barry (2012), Has the Three-Gorges Dam made the Poyang Lake wetlands wetter and drier?, *Geophys. Res. Lett.*, *39*, L20402, doi:10.1029/2012GL053431.
Zhang, Q., X.-c. Ye, A. D. Werner, Y.-l. Li, J. Yao, X.-h. Li, and C.-y. Xu (2014a), An investigation of enhanced recessions in Poyang Lake: Comparison of Yangtze River and local catchment impacts, *J. Hydrol.*, *517*, 425–434, doi:10.1016/j.jhydrol.2014.05.051.
Zhang, Q., M. Xiao, J. Li, V. P. Singh, and Z. Wang (2014b), Topography-based spatial patterns of precipitation extremes in the Poyang Lake basin, China: Changing properties and causes, *J. Hydrol.*, *512*, 229–239, doi:10.1016/j.jhydrol.2014.03.010.
Zhou, T., and R. Yu (2005), Atmospheric water vapor transport associated with typical anomalous summer rainfall patterns in China, *J. Geophys. Res.*, *110*, D08104, doi:10.1029/2004JD005413.